



## OPEN ACCESS

## EDITED BY

Bo Li,  
University of Wollongong, Australia

## REVIEWED BY

Fajin Chen,  
Guangdong Ocean University, China  
Selvaraj Kandasamy,  
Central University of Kerala, India

## \*CORRESPONDENCE

Lilei Chen,  
✉ llchen@qnlm.ac  
Duanxin Chen,  
✉ chenduanxin07@qdio.ac.cn

RECEIVED 12 June 2023

ACCEPTED 07 August 2023

PUBLISHED 17 August 2023

## CITATION

Tong G, Chen L, Zhang G, Liu J, Chen B,  
Xu G, Liu M, An Y and Chen D (2023),  
High-resolution record of temporal  
change in organic matter burial over the  
past ~8,600 years on the northwestern  
continental slope of the South China Sea.  
*Front. Earth Sci.* 11:1238920.  
doi: 10.3389/feart.2023.1238920

## COPYRIGHT

© 2023 Tong, Chen, Zhang, Liu, Chen, Xu,  
Liu, An and Chen. This is an open-access  
article distributed under the terms of the  
[Creative Commons Attribution License  
\(CC BY\)](https://creativecommons.org/licenses/by/4.0/). The use, distribution or  
reproduction in other forums is  
permitted, provided the original author(s)  
and the copyright owner(s) are credited  
and that the original publication in this  
journal is cited, in accordance with  
accepted academic practice. No use,  
distribution or reproduction is permitted  
which does not comply with these terms.

# High-resolution record of temporal change in organic matter burial over the past ~8,600 years on the northwestern continental slope of the South China Sea

Gang Tong<sup>1,2</sup>, Lilei Chen<sup>3\*</sup>, Guangxu Zhang<sup>4</sup>, Jian Liu<sup>1</sup>, Bin Chen<sup>1</sup>,  
Gang Xu<sup>1</sup>, Ming Liu<sup>5</sup>, Yuhui An<sup>5</sup> and Duanxin Chen<sup>4\*</sup>

<sup>1</sup>Qingdao Institute of Marine Geology, CGS, Qingdao, China, <sup>2</sup>School of Ocean Sciences, China University of Geosciences, Beijing, China, <sup>3</sup>Deep-sea Multidisciplinary Research Center and Laboratory for Marine Geology, Laoshan Laboratory, Qingdao, China, <sup>4</sup>Institute of Oceanology, Chinese Academy of Sciences, Qingdao, China, <sup>5</sup>College of Marine Geosciences, Ocean University of China, Qingdao, China

Sedimentary organic matter (SOM) on continental slopes in marine regions can sensitively record climatic and environmental changes. In this study, total organic carbon content (TOC), total nitrogen content (TN), and their stable isotope compositions ( $\delta^{13}\text{C}$  and  $\delta^{15}\text{N}$ ) for sediments of core G02 were investigated (at ~24.2-year resolution) to reveal the temporal variations in organic matter sources and the main controls on the sources and distribution of buried organic matter on the northwestern continental slope of the South China Sea over the last ~8600 years. Results of a  $\delta^{13}\text{C}$  binary mixing model reveal that  $\sim 82.3 \pm 3\%$  of SOM is derived from marine autochthonous sources. We suggest that the carbon and nitrogen contents and compositions of SOM are governed by distinct factors. The more positive  $\delta^{15}\text{N}$  values before the *Pulleniatina* Minimum Event occurrence are ascribed to stronger subsurface water intrusion by the Kuroshio Current, which led to enhanced subsurface denitrification and in turn counteracted the effect of mixing with surface water caused by the East Asian winter monsoon. Sedimentary  $\delta^{13}\text{C}$  values show a fluctuant decrease during ca. 8.6–3.0 cal kyr BP and a conspicuous increase during ca. 3.0–1.4 cal kyr BP. These changes are attributed to the decrease of marine productivity induced by the continuous weakening East Asian monsoon effect and the decrease of terrigenous organic carbon input induced by the weakened Indian summer monsoon precipitation, respectively. Since ca. 1.4 cal kyr BP, human activities have become the dominant factor in controlling the production and distribution of organic carbon. The results provide an important basis for understanding of source-sink processes of organic matter and the factors influencing these processes on continental slopes in low-latitude marginal seas.

## KEYWORDS

South China Sea continental slope, sedimentary organic matter, denitrification, Asian monsoon changes, human activity

# 1 Introduction

Although continental marginal seas account for only 10% of the ocean surface area, they contain more than 80% of oceanic buried organic carbon (OC) (Hedges and Keil, 1995; Allison et al., 2007; Hu et al., 2016). Sedimentary organic matter (SOM) in marginal seas comprises a complex mixture of organic compounds originating from two main sources (Hu et al., 2014; Ge et al., 2019): terrestrial organic matter (OM) transported by river runoff, and marine OM produced by marine primary producers in the euphotic zone (EZ) (Huang et al., 2021). The nature of OM that becomes buried in a marginal sea is controlled by a combination of terrestrial sediment supply, aquatic productivity, and coastal hydrodynamics (Wang et al., 2021). Determining the sources, burial process, and ultimate fate of OM in marginal sea environments is essential for

understanding regional biogeochemical processes and the global carbon cycle.

The South China Sea (SCS), the largest marginal sea of the western Pacific Ocean (Figure 1A), receives a huge amount of detritus from surrounding rivers (e.g., the Pearl, Mekong, and Red rivers) (Li et al., 2022a; Liu et al., 2023). Previous studies of the composition and distribution of sediments of the northern South China Sea (NSCS) have used element isotopes, biomarkers, and clay minerals (Liu et al., 2016; Yang et al., 2018; Chow et al., 2021). Those studies determined that sediments in the NSCS record a number of global events, including the 8.2 ka event, Last Glacial Maximum, and Younger Dryas (Wu et al., 2017; Li C. et al., 2019), suggesting a climatic teleconnection between the NSCS and the global climate system. The NSCS has the potential to provide valuable information on the strength and distribution of the Asian monsoon, the intensity of the western boundary current, and the

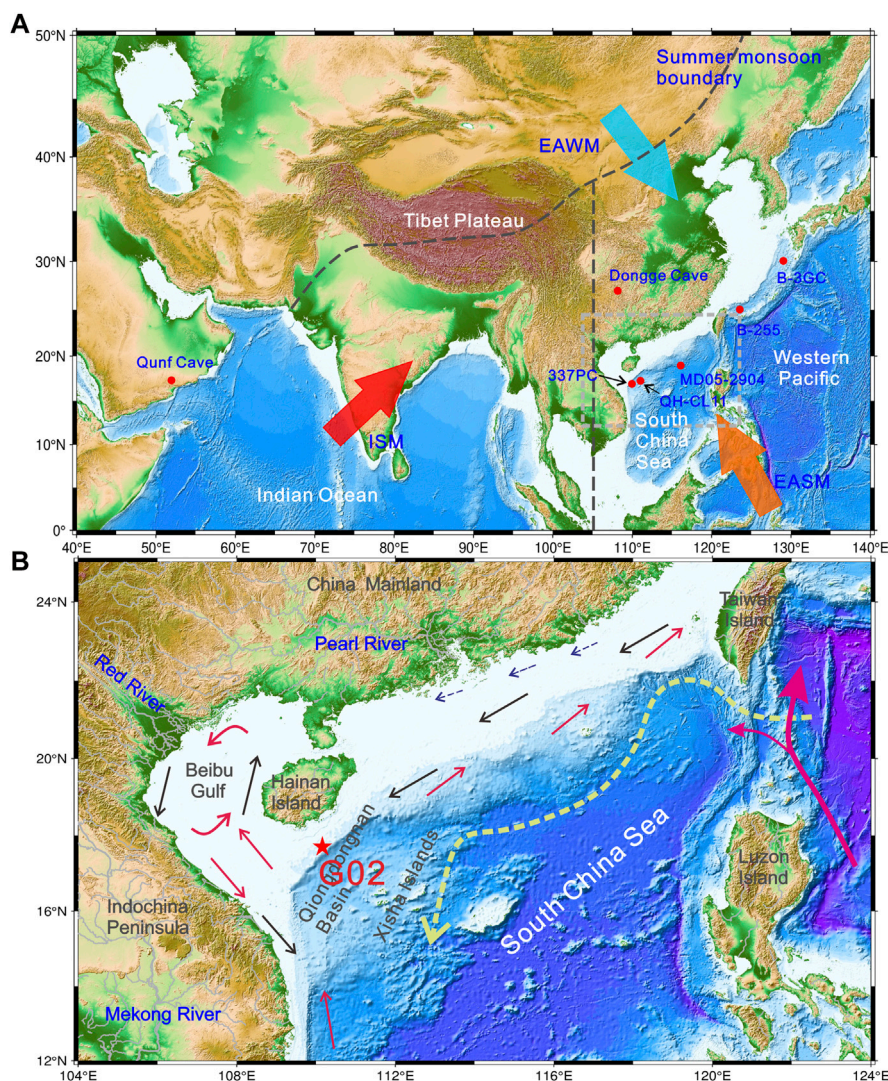


**FIGURE 1** (A) Map showing regional atmospheric systems and locations of cores in the Asian region. The blue arrow represents the East Asian winter monsoon (EAWM), the red arrow represents the Indian summer monsoon (ISM), and the orange arrow represents the East Asian summer monsoon (EASM). Red dots indicate the locations of cores referred to in this paper. (B) Topography and the main components of ocean circulation of the South China Sea (SCS). The thick red line with arrows indicates the Kuroshio Current, the dashed yellow line with the arrow depicts the SCS deep current, blue lines with arrows represent the Guangdong Coastal Current, black lines with arrows indicate winter surface currents, and red lines with arrows depict summer surface currents, red pentagram represents the location of core G02.

intrusion of the North Pacific Intermediate Water (Zheng et al., 2016; Yang et al., 2017). However, uncertainty persists regarding the cycling processes of OM in the water column, and the interpretation of paleoenvironmental records is complicated by the multitude of factors that control the nature and distribution of OM in and around the NSCS. The complex topography and dynamic transport mechanisms in the margin of the NSCS, together with heterogeneous sources of particulate organic carbon (POC), have led to pronounced temporal and spatial variations in the elemental and isotopic compositions of SOM in the NSCS. The exchange of surface water with deep water through the Luzon Strait and Taiwan Strait may have been enhanced after the opening of the Taiwan Strait (Higginson et al., 2003), resulting in an increasing influence of deep water in the NSCS. In addition, monsoonal precipitation affects river flow and alters the input of OM from terrestrial sources. Furthermore, the original marine SOM record may be complicated by post-deposition biogeochemical processes (e.g., diagenesis and denitrification). The influence of sea-level change on variation in OM burial has decreased during the Holocene, whereas the influence of ocean current systems, monsoons, and human activity has increased (Wan et al., 2015; Wu et al., 2021; Wang et al., 2022). Therefore, high-resolution SOM records are urgently needed for the NSCS.

Most geochemical studies of the NSCS have focused on the area around the Pearl River and Beibu Gulf (Lin et al., 2006; Huang et al., 2018; Zhou et al., 2022). In comparison, few systematic studies have produced high-resolution sedimentary records from the northwestern continental slope of the SCS to elucidate the sources and distribution of OM there.

In this study, we analysed core sediments from the Qiongdongnan Basin on the northwestern continental slope of the SCS (Figure 1B) for AMS  $^{14}\text{C}$  dating, grain size, total organic carbon (TOC), total nitrogen (TN),  $\delta^{13}\text{C}$ , and  $\delta^{15}\text{N}$ . Results of the analyses allow the sources of OM in sediments of the NSCS to be determined and the drivers of marine OM burial since the Holocene to be identified. The study provides insights into the relationship between OM burial and regional climate variation.

## 2 Regional setting

The SCS is the largest marginal sea in the western Pacific and is bounded by mainland China, the Indochina Peninsula, and island arcs (Figure 1B). Solar radiation received by the sea leads to a high sea surface temperature throughout the year, which generates strong vertical stratification of the water. The NSCS has a huge continental shelf that receives sediments transported by East Asian rivers such as the Pearl and Red rivers. The northern continental slope of the SCS has an important role in sediment transport and accumulation, and contains a paleoenvironmental record corresponding to its function as a connecting zone between the northern continental shelf and the central deep-sea basin of the SCS. The SCS is located in the tropical region and has a typical tropical monsoon climate influenced by the Asian monsoon (Wang et al., 1999). The surface water circulation of the SCS varies seasonally, with a seasonal surface current directed in opposite directions during summer and winter between Taiwan Island and Hainan Island. Year-round cyclonic circulation occurs in the Beibu Gulf near the Red River Estuary, in which the Qiongzhou Strait, with a westward flow of water, plays a key role. The deep-water current from the western Pacific Ocean is the only deep-water input into the SCS and reaches the deep-

sea basin east of the Xisha Islands, from where it flows southward (Liu et al., 2016). The Kuroshio intrusion has a strong influence on surface water masses in the SCS by altering temperature and salinity and contributing to the N and C biogeochemical cycles.

## 3 Materials and methods

### 3.1 Sampling

A 3.55-m-long gravity core, G02, was retrieved from the Qiongdongnan Basin in the northwestern continental slope of the SCS (17.572°N, 110.272°E, water depth of 200 m; Figure 1B) in June 2018 by Yuexia Fishery guidance ship 20026, using a gravity corer with an automatic clutch and reverse catcher. After retrieval, the core was split, described, and subsampled in the laboratory. Core G02 shows only minor along-core changes in lithology and sedimentary facies. The lithology is dominated by grey-brown clayey silt with low contents of sand-sized components. The core was subsampled into 1-cm-thick samples, which were stored immediately at  $-20^{\circ}\text{C}$  until analysis for organic geochemistry.

### 3.2 AMS $^{14}\text{C}$ dating of core sediments

Ten milligrams of planktonic foraminifera with intact shells and without black spots were selected from the  $>63\ \mu\text{m}$  fraction in core samples. These samples were shipped to the Beta Analytic Testing Laboratory (Miami, Florida, United States) for analysis. Raw radiocarbon dates were subsequently transformed into calendar ages using the Calib 8.2 calibration program, which employs the MARINE20 calibration curve (Heaton et al., 2020) with a local marine reservoir age correction ( $\Delta R = -159 \pm 49$  years).  $\Delta R$  represents the mean of three site  $\Delta R$ s from the ocean reservoir database: No. 406 (112.3°N, 16.7°E), No. 407 (112.3°N, 16.4°E), and No. 410 (106.5°N, 10.8°E). An age–depth model was constructed by Bayesian analysis using the *Undatable* program in Matlab 2016b software (Lougheed and Obrochta, 2019) (Figure 2A).

### 3.3 Grain-size analysis

Pretreatment of samples was performed prior to conducting grain-size analysis. Samples were reacted in 10%  $\text{H}_2\text{O}_2$  for 24 h to remove OM, followed by the addition of 0.5 HCl until biological carbonate was completely removed. Each sample was rinsed several times with ionized water and then treated by adding a dispersant of 0.5% sodium hexametaphosphate solution. The remaining solids were analysed using a Mastersize-2000 laser particle-size analyser. The measurement range was 0.02–2000  $\mu\text{m}$  with a size resolution of 0.01  $\mu\text{m}$ , and the measurement error was within 3% (Xu et al., 2016).

### 3.4 Analysis of organic matter

Samples were ground to a particle size of  $<75\ \mu\text{m}$  and then soaked in 0.4 mol/L HCl for 12 h at room temperature to eliminate excess inorganic carbonates. The remaining solids were rinsed four times with deionized water, freeze-dried, and transferred to tin

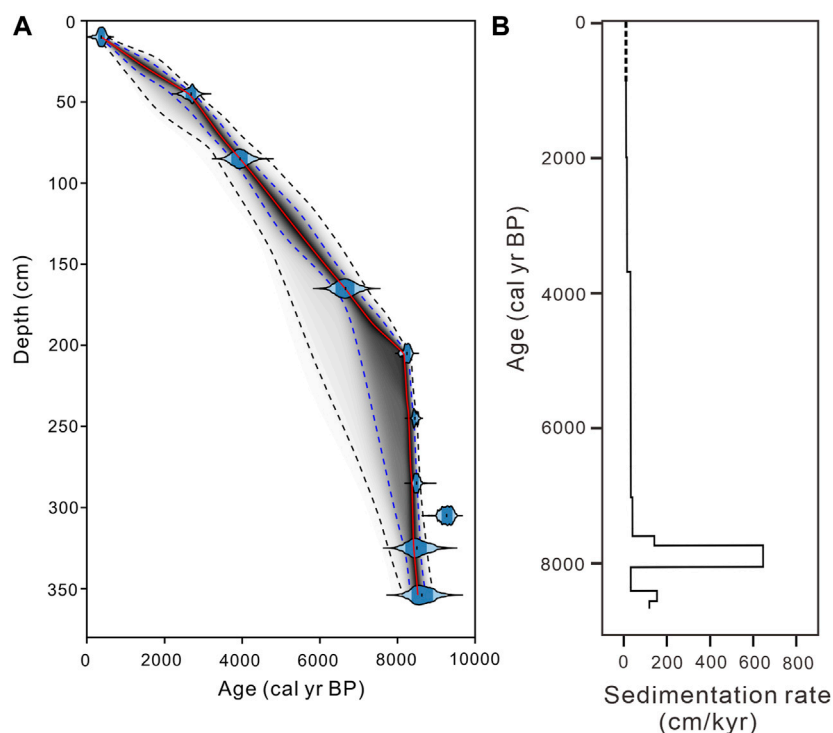


FIGURE 2

(A) Depth-age model for sediments of core G02. The shaded areas represent the  $1\sigma$  uncertainties of calendar ages obtained with Undatable software using Bayesian statistical age modelling. (B) Sedimentation rate of core G02.

TABLE 1 AMS  $^{14}\text{C}$  data from core G02.

| Depth (cm) | Material                      | AMS $^{14}\text{C}$ age (yr BP) | $1\sigma$ cal BP | Calendar age (cal yr BP) | Code no. (Beta) |
|------------|-------------------------------|---------------------------------|------------------|--------------------------|-----------------|
| 10.0       | <i>Globorotalia menardii</i>  | $1470 \pm 30$                   | 758–911          | 833                      | 528043          |
| 45.5       |                               | $3410 \pm 30$                   | 2977–3173        | 3078                     | 528044          |
| 85.0       |                               | $4290 \pm 30$                   | 4086–4292        | 4194                     | 528045          |
| 165.5      |                               | $6280 \pm 30$                   | 6408–6592        | 6502                     | 528046          |
| 205.5      |                               | $7130 \pm 30$                   | 7336–7490        | 7416                     | 528047          |
| 245.5      | Mixed planktonic foraminifera | $7390 \pm 30$                   | 7571–7723        | 7651                     | 528048          |
| 285.5      |                               | $7440 \pm 30$                   | 7617–7777        | 7701                     | 528049          |
| 305.5      |                               | $8010 \pm 30$                   | 8205–8358        | 8283                     | 541102          |
| 325.5      |                               | $8110 \pm 30$                   | 8313–8472        | 8391                     | 541103          |
| 354.5      |                               | $8290 \pm 30$                   | 8491–8696        | 8597                     | 528050          |

capsules. Analyses of TOC and TN were performed using a Euro EA 3000 elemental analyser with a standard deviation of  $\pm 0.02\%$  dry wt ( $n = 6$ ) for TOC and  $\pm 0.002\%$  dry wt ( $n = 6$ ) for TN. Analyses of stable isotopes were determined using an elemental analyser/stable isotope ratio mass spectrometer (FLASH EA 1112 series coupled with Thermo Fisher Delta V continuous flow isotopic ratio mass spectrometer) at Center for Isotope Geochemistry and Geochronology, Laoshan Laboratory with a standard deviation of  $\pm 0.1\text{‰}$  for  $\delta^{13}\text{C}$  and  $\pm 0.1\text{‰}$  for  $\delta^{15}\text{N}$  ( $n = 6$ ).

## 4 Results

### 4.1 Geochronology of core G02

AMS  $^{14}\text{C}$  dating results are presented in Table 1. Interpolation of the results indicates that the earliest (lowermost) sediments deposited in core G02 have an age of  $\sim 8.6$  cal kyr BP, with a mean sedimentation rate in the core of  $\sim 40$  cm/kyr. Overall, the calculated sedimentation rate is higher in the lower part of the core

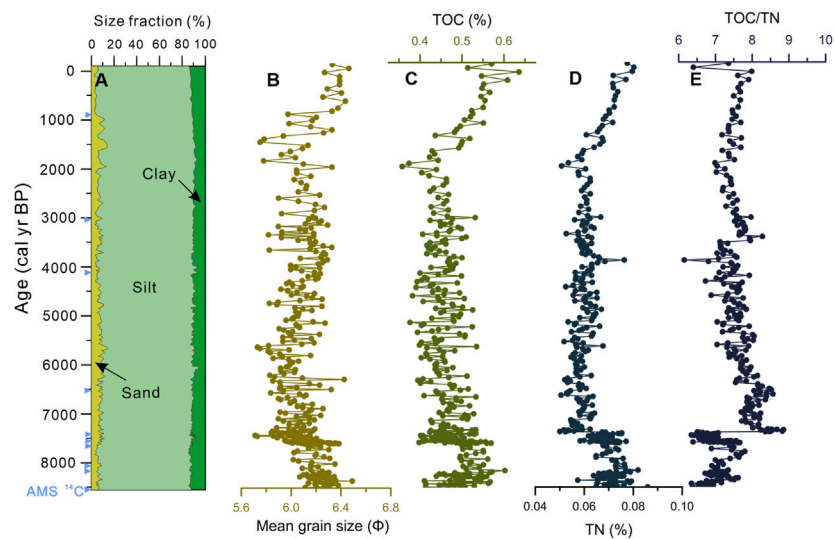


**FIGURE 3**

Temporal variations in mean grain size, sedimentary organic matter (SOM), and lithology in core G02. (A) Sediment size composition; (B) Mean grain size; (C) total organic carbon (TOC); (D) total nitrogen (TN); and (E) TOC/TN ratio.

than in the upper part. A sedimentation rate of  $\sim 180$  cm/kyr is calculated for the period 8.6–8.3 cal kyr BP. An abrupt increase in sedimentation rate is observed during 8.3–7.7 cal kyr BP, reaching  $\sim 800$  cm/kyr. After that, the sedimentation rate is stable at  $\sim 35$  cm/kyr during 7.6–4.2 cal kyr BP and decreases slightly to 15 cm/kyr after 4.2 cal kyr BP (Figure 2B).

## 4.2 Grain-size characteristics

Sediment in core G02 was mainly composed of homogeneous grey to dark-grey clayey silt, which constitutes 63.31%–88.99% of the core, with a mean value of 81.86%. The proportions of sand and clay range from 5.15% to 14.45% and from 4.96% to 14.40%, with mean values of 6.41% and 11.75%, respectively (Figure 3A; Supplementary Table S1). The mean grain size (Mz) of sediments in core G02 varies mainly from 5.8 to 6.4  $\Phi$ . The Mz showed a gradual coarsening trend from 8.6 cal kyr BP to  $\sim 5.6$  cal kyr BP due to a significant increase of sand content. Then the Mz was relatively stable (fluctuating around 6) from  $\sim 5.6$  cal kyr BP to  $\sim 1.4$  cal kyr BP followed by a slight increase of amplitude fluctuation over the last  $\sim 1.4$  kyr, there is a clear trend of refinement (Figure 3B; Supplementary Table S1).

## 4.3 Contents of organic carbon and nitrogen

Contents of TOC and TN range from 0.36% to 0.64% and from 0.05% to 0.08%, with mean values of 0.48% and 0.06%, respectively (Figures 3C, D; Supplementary Table S1). The pattern of TN content through the core is similar to that of TOC, with both being uniform in the lower part of the core and showing a small increase in the upper part. Values of  $\delta^{13}\text{C}$  and  $\delta^{15}\text{N}$  for sediments of core G02 range from  $-21.97\text{‰}$  to  $-20.63\text{‰}$  and from 5.12‰ to 6.25‰, with mean values of  $-21.20\text{‰}$  and 5.74‰, respectively (Supplementary Table

S1). Both  $\delta^{13}\text{C}$  and  $\delta^{15}\text{N}$  display multi-decadal to centennial fluctuations.  $\delta^{13}\text{C}$  values fluctuate irregularly in the bottom part of the core (355–205 cm core depth) and decrease slowly upwards from 205 to 100 cm core depth (7.3–4.6 cal kyr BP). In the uppermost 100 cm of the core,  $\delta^{13}\text{C}$  values increase sharply during 3.0–1.4 cal kyr BP and then decrease from 1.4 cal kyr BP. The most obvious feature of the  $\delta^{15}\text{N}$  values is the large fluctuations from 113 to 78 cm core depth (4.0–5.0 cal kyr BP), with substantial variation in values below and above the fluctuating interval. Values of TOC/TN for core G02 are quite uniform, ranging from 6.2 to 8.9, with a mean value of 7.4 (Figure 3E; Supplementary Table S1).

## 5 Discussion

### 5.1 Provenance of sedimentary organic matter

$\delta^{13}\text{C}$  and  $\delta^{15}\text{N}$  can be used to identify the source and distribution of OM in sediment (Selvaraj et al., 2015; Ye et al., 2017; Mackensen and Schmiedl, 2019). Because of different photosynthetic mechanisms, the stable isotope  $\delta^{13}\text{C}$  and  $\delta^{15}\text{N}$  values of OM produced by different vegetation types exhibit specific ranges, allowing the sources of OM to be traced in sediment cores (Amir et al., 2021 and references therein). Terrestrial plants are generally divided into C3 and C4 plants.  $\delta^{13}\text{C}$  values for C3 plants range from  $-30\text{‰}$  to  $-23\text{‰}$  (mean  $-27\text{‰}$ ), whereas  $\delta^{13}\text{C}$  values for C4 plants range from  $-19\text{‰}$  to  $-10\text{‰}$  (mean  $-13\text{‰}$ ).  $\delta^{13}\text{C}$  values of freshwater plants are close to those of C3 plants, generally ranging from  $-30\text{‰}$  to  $-25\text{‰}$ , and  $\delta^{13}\text{C}$  values of marine phytoplankton range from  $-22\text{‰}$  to  $-19\text{‰}$ . Similar to  $\delta^{13}\text{C}$ , TOC/TN ratios have been used to differentiate the sources of OM. Terrestrial plants contain large amounts of lignin and cellulose, resulting in higher TOC/TN ratios in comparison with marine plants. In general, TOC/TN ratios of C3 plants exceed 15 and TOC/TN ratios of C4 plants exceed 30. OM produced by marine plants has TOC/TN ratios of  $<8$ . In addition, bacterial activity

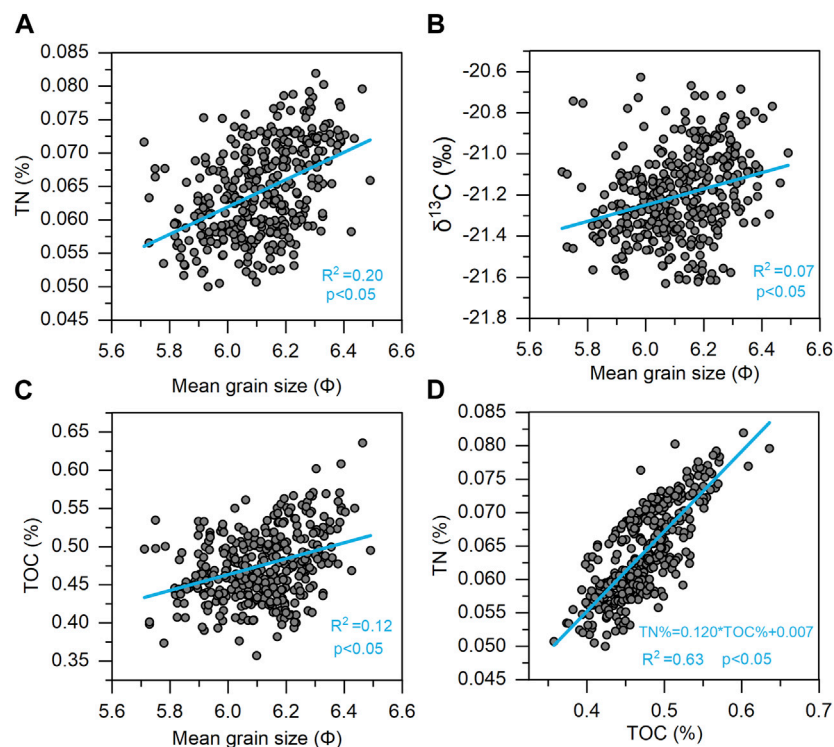


FIGURE 4

Correlation plots for (A) TN vs. mean grain size, (B)  $\delta^{13}\text{C}$  vs. mean grain size, (C) TOC vs. mean grain size, (D) TN vs. TOC.

can alter TOC/TN ratios by introducing more nitrogen into sediment, with TOC/TN ratios in areas of higher bacterial abundance typically ranging from 4 to 6 (Lamb et al., 2006; Lu et al., 2021).

Controls on the fractionation of C isotopes and on TOC/TN ratios include early diagenesis, clay sorption, and sediment grain size. Fine-grained minerals have a greater ability to adsorb OM owing to their larger specific surface area, and therefore TOC and TN contents are higher in fine- rather than coarse-grained sediments (Zhang et al., 2022).  $\delta^{13}\text{C}$  also varies according to grain-size fraction, and the stable isotope content of the fine-grained fraction is markedly higher than that of the coarse-grained fraction (Kienast et al., 2005). A plot of Mz values of sediment in core G02 versus TOC, TN and  $\delta^{13}\text{C}$  values (Figures 4A–C) reveals substantial scatter, suggesting that sediment Mz has minimal or no effect on TOC,  $\delta^{13}\text{C}$  and is only marginally correlated with TN. The use of TOC/TN ratios of SOM to determine the sources of OM in coastal settings requires consideration of the potential interference of inorganic nitrogen that is adsorbed by clay minerals in the form of  $\text{NH}_4^+$  during deposition, which leads to below-normal TOC/TN ratios. The linear correlation between TOC and TN in core G02 does not have a significant positive TN intercept (Figure 4D), suggesting that inorganic nitrogen may not be an important contribution and that TN more likely reflects the predominant contribution of organic N. In turn, this indicates that the small amount of inorganic nitrogen adsorbed by clay minerals is not sufficient to influence the source identification of SOM. It is generally accepted that  $\delta^{13}\text{C}$  is more conservative than TOC/TN ratios in the identification of sources of OM (Hu et al., 2012; Liu et al., 2023). Although early diagenesis has some influence on TOC/TN ratios, the combination of  $\delta^{13}\text{C}$  values and TOC/TN ratios has been effectively applied to constrain OC sources (Liu et al., 2023).

Both  $\delta^{13}\text{C}$  values and TOC/TN ratios of core G02 are consistent with the characteristics of marine OM. The distribution of sample data in diagrams of  $\delta^{13}\text{C}$  vs. TOC/TN ratio and  $\delta^{13}\text{C}$  vs.  $\delta^{15}\text{N}$  further indicate that the source of SOM from core G02 was a mixture of *in situ* generated marine OM and imported terrestrial OM, with a dominant marine authigenic source and a minor amount of terrestrial OM from C3 plants and freshwater phytoplankton (Figures 5A, B). This mixed source appears to reflect the typical pattern of OM distribution in the continental slope; i.e., compared with the continental shelf, the continental slope is further from the estuary and the transport of terrestrial OM to the continental slope is more difficult, meaning that terrestrial OM accounts for a smaller proportion of the core sediment. On the basis of previous studies of the northwestern SCS continental slope, it is hypothesized that terrestrial OM on this continental slope is sourced mainly from the Red River (Wan et al., 2015; Li et al., 2022b). This interpretation is supported by the Red River being the main source of sediments on the northwestern SCS continental slope, and that Red River sediment can be transported to the southeastern Qiongdongnan Basin under surface and gravity-flow transport (Li et al., 2022a). It is generally considered to be difficult for sediments from the Pearl River and Taiwan Island to reach the northwestern SCS owing to the long distance involved, and only small amounts of sediment are transported to the sea from Hainan Island on account of the absence of large rivers on the island (Li et al., 2022a). Combining the above evidence, we consider that the terrestrial OM in core G02 originated predominantly from the Red River.

To obtain a more accurate understanding of the relative proportions of OM derived from marine and terrestrial sources and their temporal trends, quantitative estimation was performed using a  $\delta^{13}\text{C}$  binary mixing model. Such models are commonly

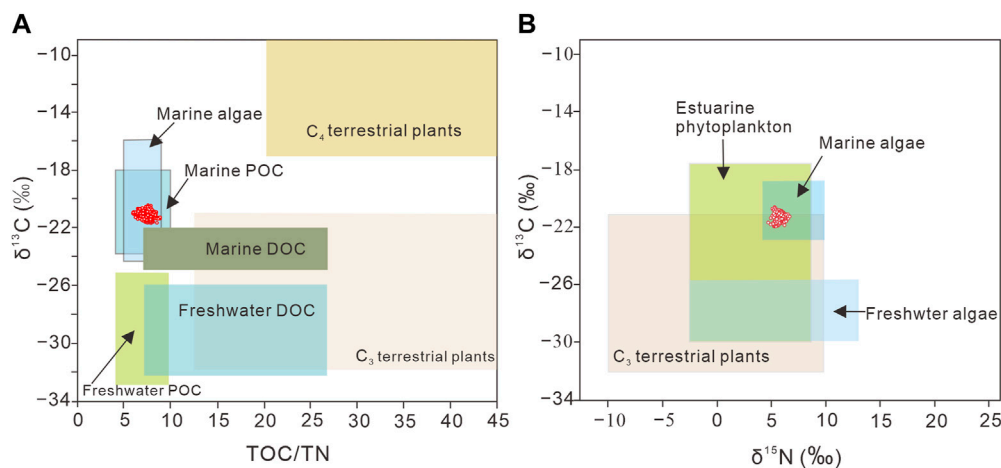


**FIGURE 5**

Organic matter (OM) source discrimination plots. (A)  $\delta^{13}\text{C}$  vs. TOC/TN; (B)  $\delta^{13}\text{C}$  vs.  $\delta^{15}\text{N}$ . Red circles depict core G02 samples from this study. Reference values for various end-members are from [Goñi et al. \(2003\)](#), [Lamb et al. \(2006\)](#), [Xia et al. \(2015\)](#), [Ho et al. \(2021\)](#), and references therein. (POC and DOC denote particulate organic carbon and dissolved organic carbon, respectively).

utilized in studies of marginal seas to estimate the ratio of OM derived from terrestrial sources ( $\text{OC}_T$ ) to OM derived from marine ( $\text{OC}_M$ ) sources ([Selvaraj et al., 2015](#); [Chen et al., 2017](#); [Zhou et al., 2022](#); [Liu et al., 2023](#)). The formulation is as follows:

$$\delta^{13}\text{C} = f_M \times \delta^{13}\text{C}_M + f_T \times \delta^{13}\text{C}_T$$

$$f_M + f_T = 1$$

where  $f_M$  and  $f_T$  represent the ratios of marine and terrestrial OC within TOC, respectively.

The global average  $\delta^{13}\text{C}$  value of the ocean and oceanic phytoplankton ( $\sim -20\text{‰}$ ) is commonly used as the marine OC endmember ([Yu et al., 2021](#)) and was also adopted in this study. Considering that the Red River serves as the primary material source in the northwestern SCS continental slope. Thus, the  $\delta^{13}\text{C}$  value of  $-26.8\text{‰}$  for surface sediments of rivers on the Red River Delta was selected as the terrestrial OC endmember ([Tue et al., 2019](#)).

The binary model analysis shows that from 8.6 cal kyr BP, the proportion of marine OM ranged from 76.0% to 90.8%, with a mean of 82.3%. From 8.6 to 3.0 cal kyr BP, there was an overall increase in terrestrial input. During 3.0–1.4 cal kyr BP, a sharp decline occurred in the proportion of terrestrial-derived OM, with levels decreasing from 23.6% to 9.2%. From 1.4 cal kyr BP, the proportion of marine autochthonous OM decreased and the proportion of terrestrial OM input showed a slight increase.

## 5.2 Influence of subsurface water intrusion on $\delta^{15}\text{N}$ values of sediments in the NSCS

### 5.2.1 Potential factors affecting $\delta^{15}\text{N}$ values in sediment

The  $\delta^{15}\text{N}$  value of sediment is highly sensitive to the oceanic nitrogen cycle and can be used to study the process of nitrogen cycling and its controlling mechanisms in the ocean ([Gaye et al., 2009](#); [Ren et al., 2012](#)). The supply of nitrogen from various external

and internal sources into the EZ, such as atmospheric nitrogen deposition, upwelling, lateral intrusion, and remineralization, modulates the biogeochemical of oligotrophic oceans and complicates nitrogen dynamics in the upper water column ([Yang et al., 2017](#); [Li M. et al., 2019](#)). If OM is well-preserved in the sediment, dynamics of nitrogen can leave distinguishable signatures in the time series of the  $\delta^{15}\text{N}$  values. Sediment  $\delta^{15}\text{N}$  values during the Middle Holocene are higher than those of the Late Holocene ([Figure 6H](#)). The variations in  $\delta^{15}\text{N}$  values within core G02 may be a function of several independent factors, such as variations in sediment grain size, diagenesis, nitrate isotopic composition, the degree of nitrate utilization, and denitrification ([Altabet, 2001](#); [Wang et al., 2022](#)).

Our analyses reveal that the variation in grain size within core G02 is negligible and that it bears no correlation to changes in  $\delta^{15}\text{N}$  ( $R^2 = 0.02$ ,  $p < 0.05$ ). Therefore, the variability in  $\delta^{15}\text{N}$  values cannot be attributed to variation in particle size. Selective degradation of OM during early diagenesis can change the nitrogen isotope signals of OM. This phenomenon is typically more pronounced in environments with lower sedimentation rates, such as the open ocean ([Tesdal et al., 2013](#)). In the present study, core G02 records a shallow water depth of 200 m and a high sedimentation rate of 40 cm/kyr. In this case, the N isotopic signatures of OM can be preserved in sediments with little isotopic alteration during sinking through the water column and subsequent burial. Therefore, in our analysis and interpretation of the  $\delta^{15}\text{N}$  variation in the core, we ignore the potential influence of early diagenesis during sedimentation ([Yang et al., 2017](#)).

The utilization of nitrate in seawater has a substantial influence on  $\delta^{15}\text{N}$  values. The assimilation of nutrients by phytoplankton preferentially uses the lighter nitrogen isotope ( $^{14}\text{N}$ ), owing to the Rayleigh fractionation effect, and  $^{15}\text{NO}_3^-$  is utilized only when  $^{14}\text{NO}_3^-$  is deficient ([Altabet, 2001](#)). In seawater with sufficient nitrate or strong upwelling, it is difficult for phytoplankton to fully utilize  $^{14}\text{NO}_3^-$ , resulting in negative  $\delta^{15}\text{N}$  values in sediments ([Gaye et al., 2013](#)). Previous studies have found that

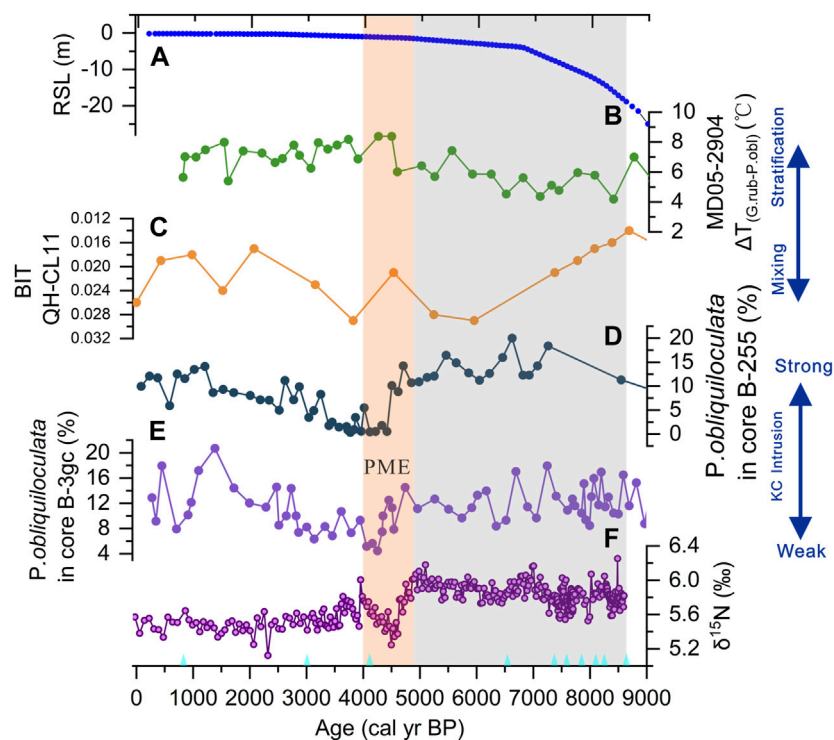


**FIGURE 6**

Comparison of results for core G02 with those of other environmental proxies. The gray bar and orange bar represent periods of enhanced and weakened Kuroshio Current (KC) intrusion, respectively. (A) Global relative sea level (RSL) (Lambeck et al., 2014); (B) The water temperature difference between layers ( $\Delta T_{(G-P)}$ ) of core MD05-2904 (Steinke et al., 2011); (C) The ratio of brGDGTs to isoGDGTs (BIT) results (Wang et al., 2023b); (D–E) abundance of *P. obliquiloculata* in cores B-3gc and B-255 (Jian et al., 2000); and (F) temporal variation in  $\delta^{15}\text{N}$  within core G02 (this study). PME = *Pulleniatina* Minimum Event.

the SCS constitutes a typical oligotrophic oceanic regime and that nitrate is an important limiting control on primary productivity in this sea (Lin et al., 2010; Yan et al., 2022). Hence, nitrate in the NSCS is generally considered to be completely depleted (Takahashi and Hori, 1984; Kienast, 2000; Liu et al., 2020). Consequently, nitrate utilization is unlikely to have regulated the variation in sediment  $\delta^{15}\text{N}$  values in core G02.

In nitrate-depleted water, nitrate in the EZ is almost completely consumed, and phytoplankton are unable to distinguish between  $^{14}\text{NO}_3^-$  and  $^{15}\text{NO}_3^-$ . The  $\delta^{15}\text{N}$  value of OM is governed primarily by the isotopic composition of nitrate in seawater rather than by the nitrogen isotopic fractionation that occurs during phytoplankton uptake (Higginson et al., 2003). Recent research conducted in the NSCS has revealed similar  $\delta^{15}\text{N}$  values for nitrate in the EZ and subsurface layer, demonstrating that subsurface nitrate serves as the primary source of new N to support export production (Yang et al., 2017). The nitrogen isotopic signature of upwelled nitrate in the subsurface may become imprinted on settling particulate organic matter that is ultimately buried in sediment (Yang et al., 2022). This altered nature of subsurface water may explain the variation in  $\delta^{15}\text{N}$  values of core G02 sediments. Denitrification reactions facilitated by denitrifying bacteria are known to influence the  $\delta^{15}\text{N}$  values of subsurface water (Yang et al., 2017). Denitrification is the process by which heterotrophic bacteria convert  $\text{NO}_3^-$  to  $\text{NO}_2^-$  or  $\text{N}_2$  under anaerobic conditions and leads to an increase in  $\delta^{15}\text{N}$  values of nitrate in seawater (Li C. et al., 2019). Denitrification is promoted by

conditions of higher TOC content, warmer temperature, lower dissolved oxygen, and lower salinity (Kienast, 2000; Guo et al., 2020). Subsurface water in the NSCS is characterized by anoxia and relatively high nitrate content, favouring the occurrence of bacterial denitrification (Yang et al., 2017; Jurikova et al., 2022). Numerous studies have demonstrated that *in situ* denitrification is responsible for the depletion of dissolved nitrate and the corresponding high  $\delta^{15}\text{N}$  values in subsurface hypoxic water (e.g., Chen et al., 2019; Yan et al., 2022). Therefore, we infer that the variation in  $\delta^{15}\text{N}$  values in core G02 sediments may have been caused by stronger subsurface water denitrification during the Middle Holocene and weaker denitrification during the Late Holocene. It is worth noting that anaerobic ammonia oxidation is coupled to denitrification and may have the same effect on  $\delta^{15}\text{N}$  (Wu et al., 2020), which needs to be further investigated in the future.

### 5.2.2 Response of sedimentary $\delta^{15}\text{N}$ values to lateral intrusion of the Kuroshio

Here, we explore the specific drivers of temporal changes in denitrification in the study area. A previous study of the Arabian Sea has shown that the decrease in sediment  $\delta^{15}\text{N}$  associated with denitrification is the low dissolved oxygen concentrations in subsurface waters, with specific mechanisms related to vertical convection between surface water and subsurface waters (Banakar et al., 2005). Strong thermoclines and haloclines prevent the vertical mixing of water, making it difficult for oxygen-rich water to be

transported downwards from the surface layer (Chen et al., 2019). Winter monsoon controlled sea surface temperature (SST) and wind strength are the main factors affecting the exchange of surface and subsurface seawater. Strong East Asian winter monsoon (EAWM) increases the depth of the mixed layer, thickens the thermocline and halocline, enhances vertical mixing of surface and subsurface seawater, and increases dissolved oxygen concentrations in the subsurface layer. Weak EAWM leads to shallower thermocline and halocline depth, weak vertical mixing and stronger stratification (Steinke et al., 2010; Zhang et al., 2022). The lack of large-scale upwelling in the northwestern SCS, where seawater stratification is common, suggests that it is possible that the variation in  $\delta^{15}\text{N}$  values in sediments of core G02 has been at least partly controlled by the upper water column stratification (Lin et al., 2010; Wu et al., 2017; Zhu et al., 2020; Wang et al., 2023a). A recent study has reconstructed the upper vertical structure of the SCS during the Holocene using  $\Delta T$  (water temperature difference between layers) and BIT index (the ratio of brGDGTs to isoGDGTs) (Wang et al., 2023b). A decrease in  $\Delta T$  and an increase in the BIT index indicate enhanced stratification (Figures 6B, C), as has been identified for the Late Holocene in the NSCS (Steinke et al., 2011). The inferred increase in stratification would have led to a positive shift in  $\delta^{15}\text{N}$  during the Late Holocene, which contradicts our results for core G02. This suggests that other factors have influenced the intensity of seawater denitrification in the subsurface water of the NSCS during 7.3–4.8 cal kyr BP, which exceeded the variation in  $\delta^{15}\text{N}$  caused by ventilation between the upper and lower water layers.

Besides vertical surface and subsurface ventilation, lateral intrusion can also affect denitrification. Bulk sediment  $\delta^{15}\text{N}$  records from modern water column denitrification zones like the eastern tropical Pacific show strong links between hydrography and denitrification rates (Dubois et al., 2011). Hydrographic variability in the NSCS is influenced predominantly by the western Pacific Ocean (Du et al., 2021; Yang et al., 2022). In particular, the nature of the surface and subsurface waters of the NSCS depends on the intensity of intrusion of the Kuroshio Current through the Luzon Strait (Liu et al., 2016). The lateral intrusion of the Kuroshio Current affects heat and salinity in the SCS, and also the biogeochemical cycling of N and C owing to the low salinity and high content of dissolved OC in Kuroshio water (Yan et al., 2022). Although few studies have examined the evolution of the Kuroshio intrusion in the NSCS, especially regarding the intensity and location of the intrusion (Du et al., 2021; Yang et al., 2022), it has been shown that the geochemical record of northern continental slope of the SCS is strongly influenced by the intensity of the Kuroshio (Li et al., 2021; Wang et al., 2023a). Records from cores B-3gc and B-255 from the western Pacific Ocean show a pronounced increase in the abundance of the planktonic foraminifer *P. obliquiloculata*, a marker species of the Kuroshio Current, at 7.3 cal kyr BP, followed by an abrupt decrease at ~4.6 cal kyr BP—Termed as the *Pulleniatina* Minimum Event (Figures 6D, E; Jian et al., 2000). In addition, Du et al. (2021) reported a westward shift and intensification of the Kuroshio Current in the Middle Holocene. A marked positive shift in  $\delta^{15}\text{N}$  values is recorded in our core G02 before ~4.8 cal kyr BP (Figure 6H), which coincides with enhanced Kuroshio intrusion, and  $\delta^{15}\text{N}$  values become negative for the period 4.8–4.2 cal kyr BP, corresponding to weakening of the SCS branch of the Kuroshio

Current intrusion. These results suggest a causal link between intrusion of the Kuroshio Current and variations in  $\delta^{15}\text{N}$ .

Intrusion of the Kuroshio Current into the NSCS occurs predominantly as subsurface water, with minimal surface water intrusion (Xu et al., 2018). In contrast to the high level of dissolved oxygen in the subsurface layer of the NSCS, the Kuroshio Current has very low levels of dissolved oxygen in the subsurface layer (Hosoda et al., 2021). Before 4.8 cal kyr BP, the intrusion of the high-salinity, low-oxygen Kuroshio Current into the NSCS intensified, reducing the dissolved oxygen concentration of NSCS subsurface water over the northwestern continental slope of the SCS via exchange. In addition, the nitrate supplied by the current resulted in an increase in the abundance of denitrifying bacteria. Although vertical ventilation may be stronger during this period compared with 4.8–0 cal kyr BP, the more pronounced Kuroshio intrusion is inferred to have led to higher  $\delta^{15}\text{N}$  values in NSCS subsurface water and therefore also affected the sediment nitrogen isotope composition. Unfortunately, few studies have examined subsurface nitrate in the SCS branch of the Kuroshio Current. Further seasonal field studies on water column nitrate and its stable isotope composition should be conducted to determine the spatial variations in nitrate isotope compositions and the exact mechanisms by which invasion of the Kuroshio Current influences the biochemical cycling of nitrogen in the NSCS.

### 5.3 Control of variation in $\delta^{13}\text{C}$ by the monsoon

Previous research on the SCS has revealed that the geochemical record of OC during glacial-interglacial cycles is primarily influenced by climate change manifested by variations in monsoon intensity, on shorter time scales, the interannual variability is predominantly attributed to changes in upwelling and circulation strengths, which are primarily associated with the monsoon and El Niño (Liu et al., 2002). The composition of OC in the marginal marine environment is governed by the relative proportions of contributions from terrestrial and marine sources (Yang et al., 2011).  $\delta^{13}\text{C}$  exhibits a fluctuating but negative trend in core G02 after ~8.6 cal kyr BP, indicating an increase in the proportion of terrestrial OC or a decrease in the proportion of marine OC. Since 8.6 cal kyr BP, the NSCS has undergone minimal sea-level change (Zong, 2004), effectively ruling out the possibility of sea-level-induced changes in terrestrially sourced input. In addition, the Mz of core G02 did not change significantly during the Middle Holocene, suggesting little change in the transport capacity of currents. We hypothesize that the changes occurring after 8.6 cal kyr BP are more likely to be influenced by monsoon variations, as inferred from various paleoclimate records from monsoonal regions elsewhere. There are two monsoon-related possibilities to explain these changes: increased OM inputs to the river and a decrease in marine biomass production.

The productivity of tropical marine areas is primarily controlled by the supply of nutrients in the upper layer of seawater. In regions with higher average water temperatures, the thicker thermocline makes it difficult for nutrients to reach the upper layer of seawater, thereby reducing marine productivity. In areas with more pronounced seasonal variations, the lower SST in winter weaken

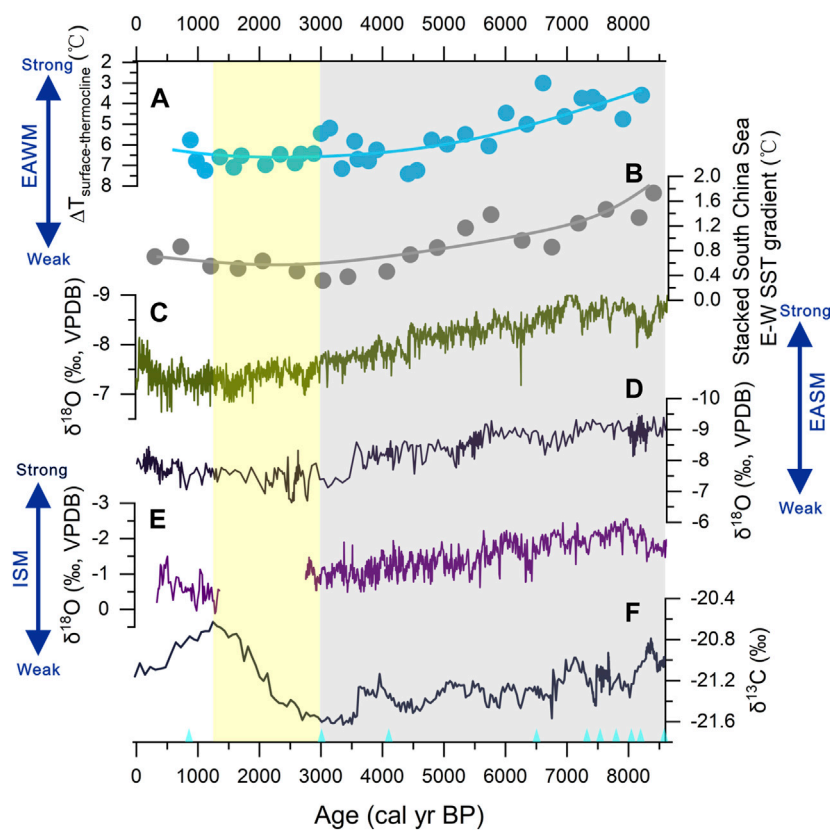


**FIGURE 7**

Comparison of EAWM, EASM and ISM proxy records with  $\delta^{13}\text{C}$  records from GO2 cores during the last 8.6 cal kyr BP. (A–B) EAWM proxies in South China Sea including SST gradient between west and east (Huang et al., 2011) and between surface and thermocline waters (Steinke et al., 2011); (C)  $\delta^{18}\text{O}$  record of Dongge Cave stalagmite (Dykoski et al., 2005); (D)  $\delta^{18}\text{O}$  record of Dongge Cave stalagmite (Wang et al., 2005); (E)  $\delta^{18}\text{O}$  of Qunf Cave stalagmite (Fleitmann et al., 2003); and (F)  $\delta^{13}\text{C}$  vs. depth for core G02.

the stratification of seawater, leading to algal blooms. Therefore, changes in temperature can affect the structure of seawater and subsequently impact marine productivity (Ge et al., 2019). Additionally, surface wind patterns can also influence the structure of the upper water column. Generally, higher wind speeds at the sea surface result in stronger mixing of seawater, leading to higher primary productivity (Li et al., 2021). Marine primary productivity in the NSCS has obvious seasonal characteristics. Liu et al. (2002) using SeaWiFS data and shipboard data revealed that the primary production of the whole basin has a strong peak in winter and a slightly weaker peak in summer, which is mainly controlled by the EAWM and East Asian summer monsoon (EASM).

Variations in the strength of the Holocene EAWM and EASM on multiple time scales have been investigated using various records, including marine sediments, stalagmites, and lake sediments (Jing et al., 2009; Wang et al., 2010; Sandeep et al., 2017; Band et al., 2018; Li et al., 2018; Li et al., 2022). Huang et al. (2011) found that the EAWM has weakened significantly since the Holocene, using the east-west SST gradient record from the NSCS (Figure 7A); Steinke et al. (2011) reached the same conclusion using the SST gradient between surface and thermocline waters (Figure 7B). The stalagmite  $\delta^{18}\text{O}$  record from Dongge Cave shows that a long-term gradual weakening of the EASM intensity starting at around 8.0 cal kyr BP

(Figures 7C, D; Dykoski et al., 2005; Wang et al., 2005). In a word, since the Holocene, especially since the Middle Holocene, both EAWM and EASM have shown a weakening trend. We therefore suggest that the decrease in the proportion of marine OC before ca. 3.0 cal kyr BP is related to the decline in marine primary productivity under East Asian monsoon control.

The decrease in  $\delta^{13}\text{C}$  continued until approximately 3.0 cal kyr BP and was followed by a rapid increase in  $\delta^{13}\text{C}$  values during 3.0–1.4 cal kyr BP. The pronounced increase in  $\delta^{13}\text{C}$  suggests an increase in the proportion of marine OM and a corresponding decrease in the contribution of terrestrial OM during this period. By this time, the EAWM have stabilised, so marine productivity is unlikely to be the main cause of the decline in the proportion of OC from terrestrial sources. The summer monsoon was still in a weakening phase (Huang et al., 2016; Huang et al., 2018), and indeed many studies suggest that it was not until 5.1 cal kyr BP that the Indian summer monsoon began to weaken at an accelerated rate (Fleitmann et al., 2003; Kohn, 2010; Chen et al., 2015; Griffiths et al., 2020). We believe that the decrease in monsoon precipitation due to the continued weakening of the summer monsoon led to a decrease in the flow of the Red River, which affected the transport of Red River material to the ocean and further led to a decrease in the proportion of terrestrial OC, which was also reflected in the sediment sedimentation rate.

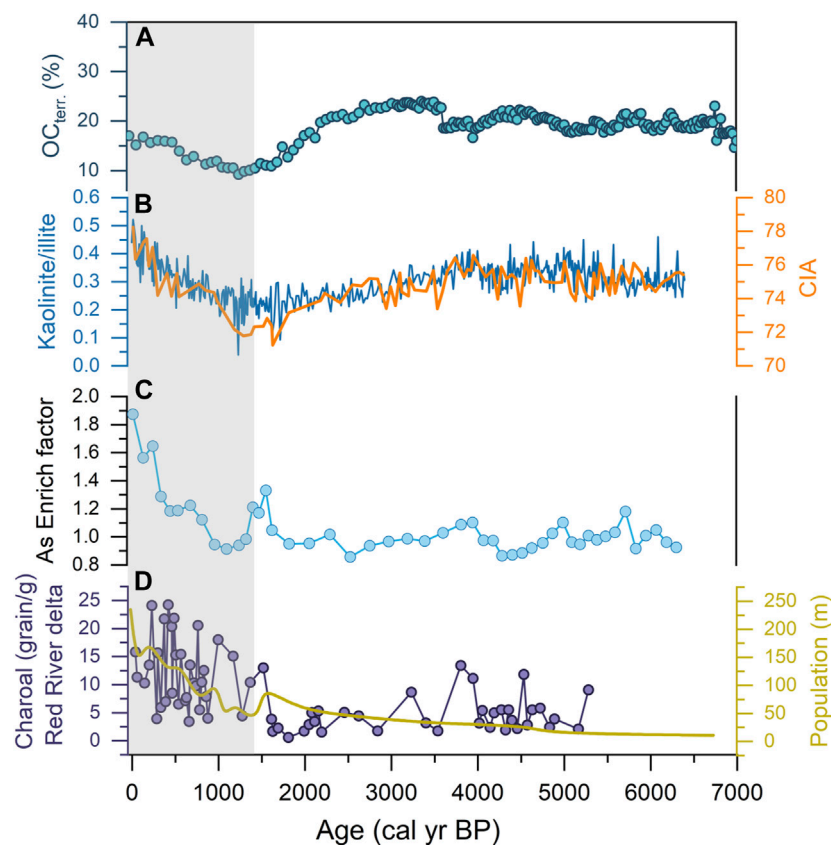


FIGURE 8

Comparison of the record of core G02 with other records for the period since 7000 cal yr BP. The vertical gray band indicates the period dominated by human activity. (A) Temporal variation of the proportion of terrestrial organic carbon in TOC in core G02; (B) chemical index of alteration (CIA) (orange line) and kaolinite/illite (K/I) (blue line) of cores from the terrestrial northwestern Southeast Qiong basin (Wan et al., 2015); (C) enrichment (enrich) factor of As for core 337PC from the northwestern Southeast Qiong basin (Wan et al., 2015); and (D) pollen record of the Erhai Sea (Shen et al., 2006) (purple points and line) and temporal change in the population of ancient/historical China (Li et al., 2009b) (yellow line).

## 5.4 Human disturbance over the past 1400 years

The negative shift in the trend of  $\delta^{13}\text{C}$  values in the Late Holocene part of core G02 and the marked increases in TOC and TN content are interpreted as reflecting an increase in the input of terrestrial OM. Results based on the binary mixing model show that the proportion of terrestrial OC starts to increase after about 1.4 cal kyr BP, increasing from 9.2% to 17.2% of TOC (Figure 8A). A significant weakening trend in the Indian summer monsoon during the Late Holocene has been identified by several studies using data from lake sediments, stalagmites, and other proxies (Fleitmann et al., 2003; Wang et al., 2005; Chen et al., 2015), implying that the increase in terrestrial OC at that time cannot be attributed to strong monsoonal precipitation.

Over the past ~1.4 kyr, temporal variation in terrestrial OC content is consistent with temporal patterns of the chemical index of alteration, the kaolinite/illite ratio, the charcoal record from the Red River delta, and the population in ancient China (Figures 8B, D). We interpret that human activity dominated the variation in input of terrestrial OM after 1.4 cal kyr BP. The population increased steadily during the Late Holocene, and it is known from archaeological information that large-scale human migration from southern China

into the lower reaches of the Red River occurred after approximately 2.0 cal kyr BP (Li et al., 2009a; Wan et al., 2015). Prior to this time, fishing and foraging were the main modes of production, whereas the southward migration of population corresponded to the introduction of the use of iron and farming techniques that greatly increased the ability to transform natural environments, primitive agriculture characterized by slash-and-burn cultivation and shifting cultivation began to develop, and metal mining and smelting also developed in parallel, as shown by the record of sulphur-related metallic elements (e.g., As) and their enrichment factors (Figure 8C). Human activity may have affected terrestrial OC inputs in two ways. First, the exposure of rocks by deforestation, farming, and mining stimulated more intense chemical and physical weathering, with eroded products being transported as sediments into marginal seas by rivers. Second, humans may have produced more OM by growing crops, and this OM was transported to marginal seas by rivers (Strong et al., 2013; Huang et al., 2018).

It is noted that the grain size of core G02 shows a clear fining trend through the Late Holocene (Figure 3A), suggesting that the transport capacity of overland flow decreased and that the intensity of the monsoon weakened (Wang et al., 2021). Fine-grained sediments play an influential role in the transport and burial of

OM (Goñi et al., 2008; Wang et al., 2021). Accordingly, we propose that fine-grained sediments also contributed to the increase in terrestrial OM content in core G02 during the Late Holocene. The increase in terrestrially sourced OM content started to stabilize at approximately 500 cal yr BP. We speculate that this change corresponds to the effects of the Little Ice Age, a major cooling event that occurred during 550–150 cal yr BP, when temperatures reached their lowest point during the last 10,000 years (Chen et al., 2015; Fan, 2023). This event may have resulted in reduced plant growth in the Red River basin, thereby slowing the increase in terrestrial OM input, as recorded in core G02.

In summary, we interpret that the impact of human activity on OM production in the Red River basin has increased since 1.4 cal kyr BP but that climatic variation has also been influential. The relative importance of these two factors needs to be more closely investigated in future studies.

## 6 Conclusion

The high-resolution (~24.2 years) multi-proxy analyses including grain size, TOC, TN, and stable isotopes ( $\delta^{13}\text{C}$  and  $\delta^{15}\text{N}$ ) of a 355 cm sediment core (G02) collected from the northwestern continental slope of the SCS reveal the role of local or remote forcing factors in controlling  $\delta^{13}\text{C}$  and  $\delta^{15}\text{N}$  variations since the past ~8600 years. Values of  $\delta^{13}\text{C}$  and C/N indicate mixed marine and terrestrial sources of OM in the studied core. A  $\delta^{13}\text{C}$  binary mixing model reveals that the source of OM in core G02 is mainly marine OM ( $82.3 \pm 3\%$ ), with the remainder being terrestrial OM. Variations in  $\delta^{13}\text{C}$  and  $\delta^{15}\text{N}$  throughout the core are poorly correlated, suggesting that C and N isotopes respond to different factors. Through the period 8.6–4.6 cal kyr BP,  $\delta^{15}\text{N}$  values of core G02 increased substantially. After excluding several potential determinants of change in  $\delta^{15}\text{N}$  values, we infer that this change reflected an increasing degree of intrusion of low-oxygen subsurface water by the Kuroshio Current into the NSCS. The low-oxygen environment enhanced the denitrification of bacteria and resulted in positive  $\delta^{15}\text{N}$  values of SOM. The continuous weakening of the East Asian monsoon and Indian summer monsoon resulted in negative  $\delta^{13}\text{C}$  values during 8.6–3.0 cal kyr BP and positive  $\delta^{13}\text{C}$  values during 3.0–1.4 cal kyr BP in the G02 core sediments, respectively. Since 1.4 cal kyr BP, human activity has played an increasingly important role in governing OC production and burial.

## Data availability statement

The raw data supporting the conclusion of this article will be made available by the authors upon reasonable request.

## References

Allison, M. A., Bianchi, T. S., McKee, B. A., and Sampere, T. P. (2007). Carbon burial on river-dominated continental shelves: impact of historical changes in sediment loading adjacent to the Mississippi River. *Geophys. Res. Lett.* 34 (1), L01606. doi:10.1029/2006gl028362

## Author contributions

GT and LC designed the study. DC and GZ collected samples in the field. LC and YA performed experiments on particle size and isotopes. GT wrote the manuscript. JL, GX, BC, DC, and ML revised the manuscript. All authors contributed to the article and approved the submitted version.

## Funding

This work was financially supported by the National Natural Science Foundation of China (Grant Nos 41906062, 41906066, 42076070, and 42176071), Natural Science Foundation of Shandong Province, China (Grant Nos ZR2020MD069 and ZR2020MD079) and Asia Cooperation Fund (Comparative Study of Geoenvironment and Geohazards in the Yangtze River Delta and the Red River Delta).

## Acknowledgments

We thank Hongying Song from the Center for Isotope Geochemistry and Geochronology, Laoshan Laboratory, Qingdao, China, for her help in isotope analysis. We also thank Shiwen Zheng and Jingbo Chen from College of Marine Geosciences, Ocean University of China, Qingdao, China, for their assistance in planktonic foraminifera selecting and sediment grain-size analysis.

## Conflict of interest

The authors declare that the research was conducted in the absence of any commercial or financial relationships that could be construed as a potential conflict of interest.

## Publisher's note

All claims expressed in this article are solely those of the authors and do not necessarily represent those of their affiliated organizations, or those of the publisher, the editors and the reviewers. Any product that may be evaluated in this article, or claim that may be made by its manufacturer, is not guaranteed or endorsed by the publisher.

## Supplementary material

The Supplementary Material for this article can be found online at: <https://www.frontiersin.org/articles/10.3389/feart.2023.1238920/full#supplementary-material>

Altabet, M. A. (2001). Nitrogen isotopic evidence for micronutrient control of fractional  $\text{NO}_3^-$  utilization in the equatorial Pacific. *Limnol. Oceanogr.* 46 (2), 368–380. doi:10.4319/lo.2001.46.2.0368

- Amir, M., Paul, D., and Malik, J. N. (2021). Geochemistry of Holocene sediments from Chilika Lagoon, India: inferences on the sources of organic matter and variability of the Indian summer monsoon. *Quat. Int.* 599 (600), 148–157. doi:10.1016/j.quaint.2020.08.050
- Banakar, V. K., Oba, T., Chodankar, A. R., Kuramoto, T., Yamamoto, M., and Minagawa, M. (2005). Monsoon related changes in sea surface productivity and water column denitrification in the Eastern Arabian Sea during the last glacial cycle. *Mar. Geol.* 219 (2–3), 99–108. doi:10.1016/j.margeo.2005.05.004
- Band, S., Yadava, M. G., Lone, M. A., Shen, C. C., Sree, K., and Ramesh, R. (2018). High-resolution mid-holocene Indian summer monsoon recorded in a stalagmite from the kotumsar Cave, Central India. *Quat. Int.* 479, 19–24. doi:10.1016/j.quaint.2018.01.026
- Chen, F., Xu, Q., Chen, J., Birks, H. J. B., Liu, J., Zhang, S., et al. (2015). East Asian summer monsoon precipitation variability since the last deglaciation. *Sci. Rep.* 5 (1), 11186. doi:10.1038/srep11186
- Chen, F., Zhou, X., Lao, Q., Wang, S., Jin, G., Chen, C., et al. (2019). Dual isotopic evidence for nitrate sources and active biological transformation in the Northern South China Sea in summer. *PLOS ONE* 14 (1), e0209287. doi:10.1371/journal.pone.0209287
- Chen, L., Liu, J., Xing, L., Krauss, K. W., Wang, J., Xu, G., et al. (2017). Historical changes in organic matter input to the muddy sediments along the Zhejiang-Fujian Coast, China over the past 160 years. *Org. Geochem.* 111, 13–25. doi:10.1016/j.orggeochem.2017.06.003
- Chow, C. H., Shih, Y. Y., Chien, Y. T., Chen, J. Y., Fan, N., Wu, W. C., et al. (2021). The wind effect on biogeochemistry in eddy cores in the northern South China sea. *Front. Mar. Sci.* 8, 717576. doi:10.3389/fmars.2021.717576
- Du, S., Xiang, R., Liu, J., Yan, H., Sha, L., Liu, J. P., et al. (2021). Variable Kuroshio current intrusion into the northern South China Sea over the last 7.3 kyr. *Palaeogeogr. Palaeoclimatol. Palaeoecol.* 562, 110093. doi:10.1016/j.palaeo.2020.110093
- Dubois, N., Kienast, M., Kienast, S., Normandeau, C., Calvert, S. E., Herbert, T. D., et al. (2011). Millennial-scale variations in hydrography and biogeochemistry in the Eastern Equatorial Pacific over the last 100 kyr. *Quat. Sci. Rev.* 30 (1–2), 210–223. doi:10.1016/j.quascirev.2010.10.012
- Dykoski, C., Edwards, R., Cheng, H., Yuan, D., Cai, Y., Zhang, M., et al. (2005). A high-resolution, absolute-dated Holocene and deglacial Asian monsoon record from Dongge Cave, China. *Earth Planet. Sci. Lett.* 233 (1–2), 71–86. doi:10.1016/j.epsl.2005.01.036
- Fan, K. (2023). The little ice age and the fall of the ming dynasty: a review. *Climate* 11 (3), 71. doi:10.3390/cli11030071
- Fleitmann, D., Burns, S. J., Mudelsee, M., Neff, U., Kramers, J., Mangini, A., et al. (2003). Holocene forcing of the Indian monsoon recorded in a stalagmite from southern Oman. *Science* 300 (5626), 1737–1739. doi:10.1126/science.1083130
- Gaye, B., Nagel, B., Dähnke, K., Rixen, T., Lahajnar, N., and Emeis, K. C. (2013). Amino acid composition and  $\delta^{15}\text{N}$  of suspended matter in the Arabian Sea: implications for organic matter sources and degradation. *Biogeosciences* 10 (11), 7689–7702. doi:10.5194/bg-10-7689-2013
- Gaye, B., Wiesner, M. G., and Lahajnar, N. (2009). Nitrogen sources in the South China Sea, as discerned from stable nitrogen isotopic ratios in rivers, sinking particles, and sediments. *Mar. Chem.* 114 (3–4), 72–85. doi:10.1016/j.marchem.2009.04.003
- Ge, Q., Xu, D., Ye, L., Yang, K., and Yao, Z. (2019). Linking monsoon activity with river-derived sediments deposition in the northern South China sea. *J. Ocean Univ. China* 18 (5), 1098–1104. doi:10.1007/s11802-019-4155-4
- Goñi, M. A., Monacchi, N., Gisewhite, R., Crockett, J., Nittrouer, C., Ogston, A., et al. (2008). Terrigenous organic matter in sediments from the Fly River delta-clinofan system (Papua New Guinea). *J. Geophys. Res.* 113 (F1), F01S10. doi:10.1029/2006JF000653
- Goñi, M. A., Teixeira, M. J., and Perkey, D. W. (2003). Sources and distribution of organic matter in a river-dominated estuary (Winyah Bay, SC, USA). *Estuar. Coast. Shelf Sci.* 57 (5–6), 1023–1048. doi:10.1016/S0272-7714(03)00008-8
- Griffiths, M. L., Johnson, K. R., Pausata, F. S. R., White, J. C., Henderson, G. M., Wood, C. T., et al. (2020). End of green sahara amplified mid-to late Holocene megadroughts in mainland Southeast Asia. *Nat. Commun.* 11 (1), 4204. doi:10.1038/s41467-020-17927-6
- Guo, J., Wang, Y., Lai, J., Pan, C., Wang, S., Fu, H., et al. (2020). Spatiotemporal distribution of nitrogen biogeochemical processes in the coastal regions of northern Beibu Gulf, south China sea. *Chemosphere* 239, 124803. doi:10.1016/j.chemosphere.2019.124803
- Heaton, T. J., Köhler, P., Butzin, M., Bard, E., Reimer, R. W., Austin, W. E. N., et al. (2020). Marine20—the marine radiocarbon age calibration curve (0–55,000 cal BP). *Radiocarbon* 62 (4), 779–820. doi:10.1017/RDC.2020.68
- Hedges, J. I., and Keil, R. G. (1995). Sedimentary organic matter preservation: an assessment and speculative synthesis. *Mar. Chem.* 49, 137–139. doi:10.1016/0304-4203(95)00013-h
- Higginson, M. J., Maxwell, J. R., and Altabet, M. A. (2003). Nitrogen isotope and chlorin paleoproductivity records from the Northern South China Sea: remote vs. local forcing of millennial- and orbital-scale variability. *Mar. Geol.* 201 (1–3), 223–250. doi:10.1016/S0025-3227(03)00218-4
- Ho, P. C., Okuda, N., Yeh, C. F., Wang, P. L., Gong, G. C., and Hsieh, C. (2021). Carbon and nitrogen isoscape of particulate organic matter in the East China Sea. *Prog. Oceanogr.* 197, 102667. doi:10.1016/j.pocean.2021.102667
- Hosoda, S., Inoue, R., Nonaka, M., Sasaki, H., Sasai, Y., and Hirano, M. (2021). Rapid water parcel transport across the Kuroshio Extension in the lower thermocline from dissolved oxygen measurements by Seaglider. *Prog. Earth Planet. Sci.* 8 (1), 16. doi:10.1186/s40645-021-00406-x
- Hu, B., Li, J., Zhao, J., Wei, H., Yin, X., Li, G., et al. (2014). Late Holocene elemental and isotopic carbon and nitrogen records from the East China Sea inner shelf: implications for monsoon and upwelling. *Mar. Chem.* 162, 60–70. doi:10.1016/j.marchem.2014.03.008
- Hu, L., Shi, X., Bai, Y., Qiao, S., Li, L., Yu, Y., et al. (2016). Recent organic carbon sequestration in the shelf sediments of the Bohai Sea and Yellow Sea, China. *J. Mar. Syst.* 155, 50–58. doi:10.1016/j.jmarsys.2015.10.018
- Hu, L., Shi, X., Yu, Z., Lin, T., Wang, H., Ma, D., et al. (2012). Distribution of sedimentary organic matter in estuarine–inner shelf regions of the East China Sea: implications for hydrodynamic forces and anthropogenic impact. *Mar. Chem.* 142 (144), 29–40. doi:10.1016/j.marchem.2012.08.004
- Huang, C., Kong, D., Chen, F., Hu, J., Wang, P., and Lin, J. (2021). Multi-proxy reconstructions of climate change and human impacts over the past 7000 Years from an archive of continental shelf sediments off eastern Hainan Island, China. *Front. Earth Sci.* 9, 663634. doi:10.3389/feart.2021.663634
- Huang, C., Zeng, T., Ye, F., Xie, L., Wang, Z., Wei, G., et al. (2018). Natural and anthropogenic impacts on environmental changes over the past 7500 years based on the multi-proxy study of shelf sediments in the northern South China Sea. *Quat. Sci. Rev.* 197, 35–48. doi:10.1016/j.quascirev.2018.08.005
- Huang, E., Tian, J., and Steinke, S. (2011). Millennial-scale dynamics of the winter cold tongue in the southern South China Sea over the past 26 ka and the East Asian winter monsoon. *Quat. Res.* 75 (1), 196–204. doi:10.1016/j.yqres.2010.08.014
- Huang, J., Wan, S., Xiong, Z., Zhao, D., Liu, X., Li, A., et al. (2016). Geochemical records of Taiwan-sourced sediments in the South China Sea linked to Holocene climate changes. *Palaeogeogr. Palaeoclimatol. Palaeoecol.* 441, 871–881. doi:10.1016/j.palaeo.2015.10.036
- Jian, Z., Wang, P., Saito, Y., Wang, J., Pflaumann, U., Oba, T., et al. (2000). Holocene variability of the Kuroshio current in the Okinawa Trough, northwestern Pacific Ocean. *Earth Planet. Sci. Lett.* 184, 305–319. doi:10.1016/S0012-821X(00)00321-6
- Jing, Z., Qi, Y., Hua, Z., and Zhang, H. (2009). Numerical study on the summer upwelling system in the northern continental shelf of the South China Sea. *Cont. Shelf Res.* 29 (2), 467–478. doi:10.1016/j.csr.2008.11.008
- Jurikova, H., Abe, O., Shiah, F. K., and Liang, M. C. (2022). New constraints on biological production and mixing processes in the South China Sea from triple isotope composition of dissolved oxygen. *Biogeosciences* 19 (7), 2043–2058. doi:10.5194/bg-19-2043-2022
- Kienast, M., Higginson, M. J., Mollenhauer, G., Eglinton, T. I., Chen, M. T., and Calvert, S. E. (2005). On the sedimentological origin of down-core variations of bulk sedimentary nitrogen isotope ratios. *Paleoceanography* 20 (2). doi:10.1029/2004PA001081
- Kienast, M. (2000). Unchanged nitrogen isotopic composition of organic matter in the South China Sea during the last climatic cycle: global implications. *Paleoceanography* 15 (2), 244–253. doi:10.1029/1999PA000407
- Kohn, M. J. (2010). Carbon isotope compositions of terrestrial C3 plants as indicators of (paleo)ecology and (paleo)climate. *Proc. Natl. Acad. Sci.* 107 (46), 19691–19695. doi:10.1073/pnas.1004933107
- Lamb, A. L., Wilson, G. P., and Leng, M. J. (2006). A review of coastal palaeoclimate and relative sea-level reconstructions using  $\delta^{13}\text{C}$  and C/N ratios in organic material. *Earth-Science Rev.* 75 (1–4), 29–57. doi:10.1016/j.earscirev.2005.10.003
- Lambeck, K., Rouby, H., Purcell, A., Sun, Y., and Sambridge, M. (2014). Sea level and global ice volumes from the last glacial maximum to the Holocene. *Proc. Natl. Acad. Sci.* 111 (43), 15296–15303. doi:10.1073/pnas.1411762111
- Li, C., Jian, Z., Jia, G., Dang, H., and Wang, J. (2019). Nitrogen fixation changes regulated by upper water structure in the South China sea during the last two glacial cycles. *Glob. Biogeochem. Cycles* 33 (8), 1010–1025. doi:10.1029/2019GB006262
- Li, J., Dodson, J., Yan, H., Wang, W., Innes, J. B., Zong, Y., et al. (2018). Quantitative Holocene climatic reconstructions for the lower Yangtze region of China. *Clim. Dyn.* 50 (3–4), 1101–1113. doi:10.1007/s00382-017-3664-3
- Li, M., Ouyang, T., Zhu, Z., Tian, C., Peng, S., Tang, Z., et al. (2019). Rare earth element fractionations of the northwestern South China Sea sediments, and their implications for East Asian monsoon reconstruction during the last 36 kyr. *Quat. Int.* 525, 16–24. doi:10.1016/j.quaint.2019.09.007
- Li, M., Ouyang, T., Zhu, Z., Tian, C., Peng, S., Zhong, H., et al. (2022a). Reconstruction of chemical weathering intensity and asian summer monsoon evolution in the Red River basin over the past 36 kyr. *Paleoceanogr. Palaeoclimatol.* 37 (5), 4397. doi:10.1029/2021PA004397
- Li, X., Dodson, J., Zhou, J., and Zhou, X. (2009a). Increases of population and expansion of rice agriculture in Asia, and anthropogenic methane emissions since 5000 BP. *Quat. Int.* 202 (1–2), 41–50. doi:10.1016/j.quaint.2008.02.009

- Li, Y., Pérez-Mejías, C., Zhao, J., Li, H., Zhang, H., Lu, J., et al. (2022b). Indian summer monsoon variations during the Younger Dryas as revealed by a laminated stalagmite record from the Tibetan Plateau. *Quat. Sci. Rev.* 278, 107375. doi:10.1016/j.quascirev.2022.107375
- Li, Z., Pospelova, V., Liu, L., Francois, R., Wu, Y., Mertens, K. N., et al. (2021). High-resolution reconstructions of Holocene sea-surface conditions from dinoflagellate cyst assemblages in the northern South China Sea. *Mar. Geol.* 438, 106528. doi:10.1016/j.margeo.2021.106528
- Li, Z., Saito, Y., Dang, P. X., Matsumoto, E., and Vu, Q. L. (2009b). Warfare rather than agriculture as a critical influence on fires in the late Holocene, inferred from northern Vietnam. *Proc. Natl. Acad. Sci.* 106 (28), 11490–11495. doi:10.1073/pnas.0813258106
- Lin, D. C., Liu, C. H., Fang, T. H., Tsai, C. H., Murayama, M., and Chen, M. T. (2006). Millennial-scale changes in terrestrial sediment input and Holocene surface hydrography in the northern South China Sea (IMAGES MD972146). *Palaeogeogr. Palaeoclimatol. Palaeoecol.* 236 (1–2), 56–73. doi:10.1016/j.palaeo.2005.11.039
- Lin, I. I., Lien, C. C., Wu, C. R., Wong, G. T. F., Huang, C. W., and Chiang, T. L. (2010). Enhanced primary production in the oligotrophic South China Sea by eddy injection in spring. *Geophys. Res. Lett.* 37 (16), L16602. doi:10.1029/2010GL043872
- Liu, K. K., Chao, S. Y., Shaw, P. T., Gong, G. C., Chen, C. C., and Tang, T. Y. (2002). Monsoon-forced chlorophyll distribution and primary production in the South China Sea: observations and a numerical study. *Deep Sea Res. Part I Oceanogr. Res. Pap.* 49 (8), 1387–1412. doi:10.1016/S0967-0637(02)00035-3
- Liu, M., Li, C., Zhang, F., Zhang, R., Yang, W., Chen, M., et al. (2020). A persistent increase in primary productivity east off Hainan Island (northwestern South China Sea) over the last decades as inferred from sediment records. *Mar. Pollut. Bull.* 158, 111428. doi:10.1016/j.marpolbul.2020.111428
- Liu, S., Li, D. W., Xiang, R., Yu, M., Zhang, H., Li, L., et al. (2023). Intensification of the East Asian winter monsoon resulted in greater preservation of terrestrial organic carbon on the inner shelf of the East China Sea since the last 1400 years. *Palaeogeogr. Palaeoclimatol. Palaeoecol.* 615, 111454. doi:10.1016/j.palaeo.2023.111454
- Liu, Z., Zhao, Y., Colin, C., Statterger, K., Wiesner, M. G., Huh, C. A., et al. (2016). Source-to-sink transport processes of fluvial sediments in the South China Sea. *Earth-Science Rev.* 153, 238–273. doi:10.1016/j.earscirev.2015.08.005
- Lougheed, B. C., and Obrochta, S. P. (2019). A rapid, deterministic age-depth modeling routine for geological sequences with inherent depth uncertainty. *Paleoceanogr. Paleoclimatology* 34 (1), 122–133. doi:10.1029/2018PA003457
- Lu, X., Huang, C., Chen, F., Zhang, S., Lao, Q., Chen, C., et al. (2021). Carbon and nitrogen isotopic compositions of particulate organic matter in the upwelling zone off the east coast of Hainan Island, China. *Mar. Pollut. Bull.* 167, 112349. doi:10.1016/j.marpolbul.2021.112349
- Mackensen, A., and Schmiedl, G. (2019). Stable carbon isotopes in paleoceanography: atmosphere, oceans, and sediments. *Earth-Science Rev.* 197, 102893. doi:10.1016/j.earscirev.2019.102893
- Ren, H., Sigman, D. M., Chen, M. T., and Kao, S. J. (2012). Elevated foraminifera-bound nitrogen isotopic composition during the last ice age in the South China Sea and its global and regional implications. *Glob. Biogeochem. Cycles* 26 (1), 26. doi:10.1029/2010GB004020
- Sandeep, K., Shankar, R., Warrier, A. K., Yadava, M. G., Ramesh, R., Jani, R. A., et al. (2017). A multi-proxy lake sediment record of Indian summer monsoon variability during the Holocene in southern India. *Palaeogeogr. Palaeoclimatol. Palaeoecol.* 476, 1–14. doi:10.1016/j.palaeo.2017.03.021
- Selvaraj, K., Lee, T. Y., Yang, J. Y. T., Canuel, E. A., Huang, J. C., Dai, M., et al. (2015). Stable isotopic and biomarker evidence of terrigenous organic matter export to the deep sea during tropical storms. *Mar. Geol.* 364, 32–42. doi:10.1016/j.margeo.2015.03.005
- Shen, J., Jones, R. T., Yang, X., Dearing, J. A., and Wang, S. (2006). The Holocene vegetation history of Lake Erhai, Yunnan province southwestern China: the role of climate and human forcings. *Holocene* 16 (2), 265–276. doi:10.1191/0959683606hl923rp
- Steinke, S., Glatz, C., Mohtadi, M., Groeneveld, J., Li, Q., and Jian, Z. (2011). Past dynamics of the East Asian monsoon: no inverse behaviour between the summer and winter monsoon during the Holocene. *Glob. Planet. Change* 78 (3–4), 170–177. doi:10.1016/j.gloplacha.2011.06.006
- Steinke, S., Mohtadi, M., Groeneveld, J., Lin, L. C., Löwemark, L., Chen, M. T., et al. (2010). Reconstructing the southern south China sea upper water column structure since the last glacial maximum: implications for the East Asian winter monsoon development. *Paleoceanography* 25 (2), 1850. doi:10.1029/2009PA001850
- Strong, D., Flecker, R., Valdes, P. J., Wilkinson, I. P., Rees, J. G., Michaelides, K., et al. (2013). A new regional, mid-Holocene palaeoprecipitation signal of the Asian Summer Monsoon. *Quat. Sci. Rev.* 78, 65–76. doi:10.1016/j.quascirev.2013.07.034
- Takahashi, M., and Hori, T. (1984). Abundance of picophytoplankton in the subsurface chlorophyll maximum layer in subtropical and tropical waters. *Mar. Biol.* 79 (2), 177–186. doi:10.1007/BF00951826
- Tesdal, J. E., Galbraith, E. D., and Kienast, M. (2013). Nitrogen isotopes in bulk marine sediment: linking seafloor observations with subsurface records. *Biogeosciences* 10 (1), 101–118. doi:10.5194/bg-10-101-2013
- Tue, N. T., Quan, D. M., Nguyen, P. T., Dung, L. V., Quy, T. D., and Nhuan, M. T. (2019). Holocene environmental changes in Red River delta, Vietnam as inferred from the stable carbon isotopes and C/N ratios. *J. Earth Syst. Sci.* 128 (1), 15. doi:10.1007/s12040-018-1041-1
- Wan, S., Toucanne, S., Clift, P. D., Zhao, D., Bayon, G., Yu, Z., et al. (2015). Human impact overwhelms long-term climate control of weathering and erosion in southwest China. *Geology* 43 (5), 439–442. doi:10.1130/G36570.1
- Wang, H., Kandasamy, S., Liu, Q., Lin, B., Lou, J. Y., Veeran, Y., et al. (2021). Roles of sediment supply, geochemical composition and monsoon on organic matter burial along the longitudinal mud belt in the East China Sea in modern times. *Geochim. Cosmochim. Acta*, 66–86. doi:10.1016/j.gca.2021.04.025
- Wang, L., Sarnthein, M., Erlenkeuser, H., Grimalt, J., Grootes, P., Heilig, S., et al. (1999). East Asian monsoon climate during the late pleistocene: high-resolution sediment records from the South China Sea. *Mar. Geol.* 156 (1–4), 245–284. doi:10.1016/S0025-3227(98)00182-0
- Wang, L., Ye, F., Wei, G., Huang, C., Chen, F., Li, Z., et al. (2022). East Asian summer monsoon and human activity imprint on  $\delta^{15}\text{N}_{\text{org}}$  records at the northern coast of the South China Sea over the last 7500 years. *Palaeogeogr. Palaeoclimatol. Palaeoecol.* 595, 110976. doi:10.1016/j.palaeo.2022.110976
- Wang, M., Chen, X., Qin, L., Man, M., Su, M., and Jia, G. (2023a). Concomitant changes of lipid biomarker and water column mixing since mid-Holocene. *Chem. Geol.* 629, 121502. doi:10.1016/j.chemgeo.2023.121502
- Wang, X., Zhong, Y., Clift, P. D., Feng, Y., Wilson, D. J., Kaboth-Bahr, S., et al. (2023b). Interactions between depositional regime and climate proxies in the northern South China sea since the last glacial maximum. *Paleoceanogr. Paleoclimatology* 38 (3), e2022PA004591. doi:10.1029/2022PA004591
- Wang, Y., Cheng, H., Edwards, R. L., He, Y., Kong, X., An, Z., et al. (2005). The Holocene Asian monsoon: links to solar changes and North Atlantic climate. *Science* 308 (5723), 854–857. doi:10.1126/science.1106296
- Wang, Y., Liu, X., and Herzschuh, U. (2010). Asynchronous evolution of the Indian and East Asian summer monsoon indicated by Holocene moisture patterns in monsoonal central Asia. *Earth-Science Rev.* 103 (3–4), 135–153. doi:10.1016/j.earscirev.2010.09.004
- Wu, J., Hong, Y., Wen, X., Li, Y., Wang, Y., and Chang, X. (2020). Activity, abundance, and community composition of anaerobic ammonia-oxidizing (anammox) bacteria in sediment cores of the Pearl River Estuary. *Estuaries Coasts* 43 (1), 73–85. doi:10.1007/s12237-019-00668-1
- Wu, K., Shi, X., Lou, Z., Wu, B., Li, J., Zhang, H., et al. (2021). Sedimentary responses to climate changes and human activities over the past 7400 Years in the western Sunda shelf. *Front. Earth Sci.* 9, 631815. doi:10.3389/feart.2021.631815
- Wu, M. S., Zong, Y., Mok, K. M., Cheung, K. M., Xiong, H., and Huang, G. (2017). Holocene hydrological and sea surface temperature changes in the northern coast of the South China Sea. *J. Asian Earth Sci.* 135, 268–280. doi:10.1016/j.jseaes.2017.01.004
- Xia, X., Wu, Q., Zhu, B., Zhao, P., Zhang, S., and Yang, L. (2015). Analyzing the contribution of climate change to long-term variations in sediment nitrogen sources for reservoirs/lakes. *Sci. Total Environ.* 523, 64–73. doi:10.1016/j.scitotenv.2015.03.140
- Xu, G., Liu, J., Liu, S., Wang, Z., Hu, G., and Kong, X. (2016). Modern muddy deposit along the Zhejiang coast in the East China Sea: response to large-scale human projects. *Cont. Shelf Res.* 130, 68–78. doi:10.1016/j.csr.2016.10.007
- Xu, M. N., Zhang, W., Zhu, Y., Liu, L., Zheng, Z., Wan, X. S., et al. (2018). Enhanced ammonia oxidation caused by lateral Kuroshio intrusion in the boundary zone of the northern South China Sea. *Geophys. Res. Lett.* 45 (13), 6585–6593. doi:10.1029/2018GL077896
- Yan, X., Yang, J. Y. T., Xu, M. N., Tan, E., Zheng, Z., Zou, W., et al. (2022). Isotope constraints on nitrogen dynamics in the upper water column of the South China Sea. *Front. Mar. Sci.* 9, 1104135. doi:10.3389/fmars.2022.1104135
- Yang, B., Liu, S. M., and Zhang, G. L. (2018). Geochemical characteristics of phosphorus in surface sediments from the continental shelf region of the northern South China Sea. *Mar. Chem.* 198, 44–55. doi:10.1016/j.marchem.2017.11.001
- Yang, J. Y. T., Kao, S. J., Dai, M., Yan, X., and Lin, H. L. (2017). Examining N cycling in the northern South China sea from N isotopic signals in nitrate and particulate phases: n cycling in the South China sea. *J. Geophys. Res. Biogeosciences* 122 (8), 2118–2136. doi:10.1002/2016JG003618
- Yang, J. T., Tang, J., Kang, S., Dai, M., Kao, S., Yan, X., et al. (2022). Comparison of nitrate isotopes between the South China sea and western North Pacific ocean: insights into biogeochemical signals and water exchange. *J. Geophys. Res. Oceans* 127 (5), 18304. doi:10.1029/2021JC018304

- Yang, S., Tang, M., Yim, W. W. S., Zong, Y., Huang, G., Switzer, A. D., et al. (2011). Burial of organic carbon in Holocene sediments of the Zhujiang (Pearl River) and Changjiang (Yangtze River) estuaries. *Mar. Chem.* 123 (1–4), 1–10. doi:10.1016/j.marchem.2010.07.001
- Ye, F., Guo, W., Shi, Z., Jia, G., and Wei, G. (2017). Seasonal dynamics of particulate organic matter and its response to flooding in the Pearl River Estuary, China, revealed by stable isotope ( $\delta^{13}\text{C}$  and  $\delta^{15}\text{N}$ ) analyses. *J. Geophys. Res. Oceans* 122 (8), 6835–6856. doi:10.1002/2017JC012931
- Yu, M., Eglinton, T. I., Haghipour, N., Montluçon, D. B., Wacker, L., Hou, P., et al. (2021). Contrasting fates of terrestrial organic carbon pools in marginal sea sediments. *Geochimica Cosmochimica Acta* 309, 16–30. doi:10.1016/j.gca.2021.06.018
- Zhang, M., Liu, X., Xu, F., Li, A., Gu, Y., Chang, X., et al. (2022). Organic carbon deposition on the inner shelf of the East China sea constrained by sea level and climatic changes since the last deglaciation. *J. Ocean Univ. China* 2022, 1–13. doi:10.1007/s11802-023-5476-x
- Zheng, X., Kao, S., Chen, Z., Menviel, L., Chen, H., Du, Y., et al. (2016). Deepwater circulation variation in the South China sea since the last glacial maximum. *Geophys. Res. Lett.* 43 (16), 8590–8599. doi:10.1002/2016GL070342
- Zhou, G., Cao, X., Xia, J., Wang, S., and Song, Z. (2022). A dramatic marine environment change in the Beibu Gulf of the South China Sea around 3.2 kyr BP. *Lithosphere* 2022, 2632112. doi:10.2113/2022/2632112
- Zhu, X., Jia, G., Mao, S., Sun, Y., Wu, N., Tian, Y., et al. (2020). Long chain 1,14-diols as potential indicators for upper water stratification in the open South China Sea. *Ecol. Indic.* 110, 105900. doi:10.1016/j.ecolind.2019.105900
- Zong, Y. (2004). Mid-Holocene sea-level highstand along the Southeast coast of China. *Quat. Int.* 117 (1), 55–67. doi:10.1016/S1040-6182(03)00116-2